

Surface Driven Bulk Reorganization of Gold Nanorods

Yanting Wang,^a S. Teitel^a and Christoph Dellago^b

^a*Department of Physics and Astronomy, University of Rochester, Rochester, NY 14627*

^b*Institute for Experimental Physics, University of Vienna, Boltzmannngasse 5, 1090 Vienna, Austria*

Molecular dynamic simulations are used to study the structural stability of gold nanorods upon heating. We show that the global stability of the rod is governed by the free energetics of its surface. In particular, an instability of surface facets nucleates a bulk instability that leads to both surface and bulk reorganization of the rod. The surface reorganizes to form new, more stable, $\{111\}$ facets, while the underlying fcc lattice completely reorients to align with this new surface structure. Rods with predominantly $\{111\}$ facets remain stable until melting.

PACS numbers: 64.70.Nd, 61.46.+w, 82.60.Qr

The global shape of a crystal structure is in general determined by its growth process. For macroscopic sized crystals, this shape will rarely be the true *equilibrium shape* that minimizes the total free energy; slow diffusion over macroscopic length scales generally result in a bulk structure and non-equilibrium global shape that are stable on all experimental time scales. Metallic crystals of micron size, however, have been observed to take their equilibrium shape when annealed for long times at high temperatures [1]. The standard theory of equilibrium shapes [2] minimizes the surface free energy, assuming that the bulk free energy remains constant. Surfaces are assumed to be large enough that the thermodynamic limit applies, and the vanishing of a surface facet is determined by the roughening transition of the corresponding surface. It is generally assumed that the equilibrium shape is achieved by a process of surface diffusion.

For structures on the *nanometer* scale, however, where surface and bulk free energies may be comparable, such a clear division between surface and bulk effects is no longer obvious. Moreover, when surface facets are only several atoms across, it is not clear that they will behave in the same manner as macroscopically large surfaces. Recent calculations by Zhao and Yakobson [3] for silicon nanowires have explicitly decomposed the energy into bulk, surface and edge contributions, showing the importance of the surface and edge terms in determining the globally stable structure. Diao *et al.* [4], in numerical simulations of $\langle 100 \rangle$ oriented gold nanowires with small cross-sectional area ($< 4 \text{ nm}^2$), showed that the surface strain associated with $\{100\}$ facets can drive a transformation of the interior from the fcc structure that is the stable structure for macroscopic bulk gold, to a bct (body-centered-tetragonal) structure. It is therefore of great interest to study under what situations nanostructures with non-equilibrium initial shapes may become globally unstable, to identify the particular mechanism leading to the instability, and to study the resulting ki-

netic path that the system takes to achieve a more stable shape.

In this work we consider gold nanorods of low aspect ratio ~ 3 , as have been studied in recent laser heating experiments [5–8]. Using molecular dynamic (MD) simulations of a rod with a few thousand atoms, we find that the stability of the nanorod against changes in shape and bulk structure is still governed by the energetics of its surface facets. A rod covered primarily by $\{111\}$ facets remains stable up until melting. However for a rod which has a sizable fraction of its surface covered by $\{110\}$ or $\{100\}$ facets, an instability of those facets sets in well below melting and leads to a shape transformation to a shorter and wider structure. The surface reorganizes to form higher stability $\{111\}$ facets. More surprisingly, the fcc interior completely reorganizes as well, rotating to align with the new facet planes.

The initial rod configuration that we consider, shown in Fig.1, is that proposed in Ref. [5]. The interior of the rod is a pure fcc lattice. The surface of the rod consists of four large $\{100\}$ and four large $\{110\}$ facets oriented parallel to the rod axis. The ends of the rod have a $\{001\}$ facet and four small $\{111\}$ facets connecting the $\{110\}$ and the $\{001\}$ facets. These experiments found that, upon heating, such rods underwent a shape transformation to bent, twisted, shorter, wider, and “ ϕ -shaped” rods in which the middle of the rod bulges outwards. Transmission electron microscopy studies [8] observed point and planar internal defects to accompany such shape transformations. Recent MD simulations [9] of such rods, using a continuous heating procedure meant to model the laser heating of experiments, found similar shape transformations. These simulations found the shape transformation to be accompanied by a structural change in which planes of interior atoms shift, converting local fcc structure to hcp. The extent and stability of these interior rearrangements was found to depend upon both the heating rate and the number of atoms in

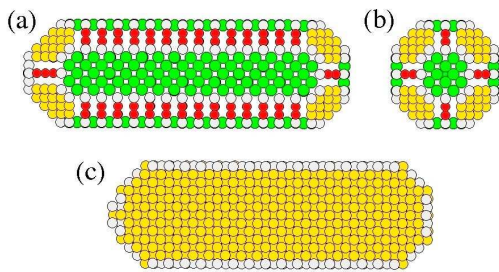


FIG. 1: Initial configuration of the gold nanorod with $N = 2624$ atoms and aspect ratio 3: (a) side view, (b) end view down the long axis, (c) cross-sectional view parallel to long axis. In (a) and (b), yellow atoms represent $\{111\}$ facets, green atoms $\{100\}$ facets, and red atoms $\{110\}$ facets; white atoms are on the edges. In (c), yellow atoms are those with a local fcc structure, white atoms are on the surface; the cross-sectional view in (c) shows atoms in the square arrangement of a $\{100\}$ plane of the fcc lattice.

the cluster, but no specific mechanism or energetic argument for this structural rearrangement was proposed. In this paper we present new simulations carried out with a much slower “quasi-equilibrium” heating that allows the rod more time to approach configurations of local equilibrium. Our results make it clear that it is the energetics of the surface that is driving the shape and structural transformation.

We use the empirical “glue” potential [10] to model the many body interactions of the gold atoms in our simulated nanorod, and we integrate the classical equations of motion for the atoms using the velocity Verlet algorithm [11] with a time step of 4.3 fs. However instead of increasing the kinetic energy at each MD step to model continuous heating as in Ref. [9], we now use the Gaussian isokinetic thermostat [12] to keep the total kinetic energy fixed at a constant temperature T ; after each MD step, all velocities are rescaled by a constant factor so as to keep $\langle(1/2)mv^2\rangle = (3/2)k_B T$ fixed. Our procedure conserves total linear and angular momentum, which are set to zero, so that our rod does not drift or rotate throughout our simulation. At each fixed T we carry out 10^7 MD steps, for a simulated time of 43 ns, before increasing the temperature in jumps of 100 K. Our effective heating rate is therefore $\sim 2.3 \times 10^9$ K/s, more than three orders of magnitude slower than the continuous heating rates of $2-7 \times 10^{12}$ K/s used in Ref. [9]. We use a rod of $N = 2624$ atoms with initial aspect ratio of 3, as shown in Fig. 1. The length of the rod, parallel to its long axis, is 7.38 nm and its cross-sectional area has a diameter of 2.46 nm. We do a short equilibration for 430 ps (10^5 MD steps) at 5 K in order to relax the surface atoms of the rod from their initial fcc positions, before starting to heat the rod.

As a signature of the shape change of our nanocluster we measure the radius of gyration, r_g , defined by $r_g^2 = (1/N) \sum_i |\mathbf{r}_i - \mathbf{r}_c|^2$, where \mathbf{r}_i is the position of atom i and

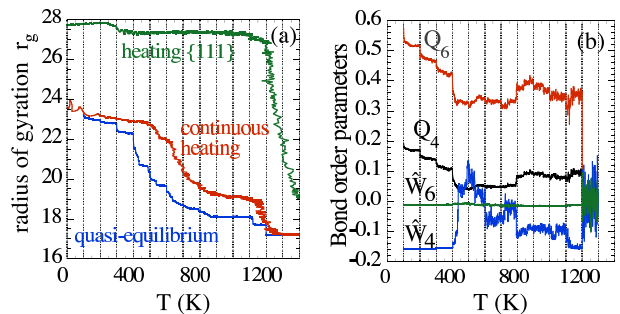


FIG. 2: (a) Radius of gyration r_g vs. temperature T for the rod of Fig. 1: quasi-equilibrium heating (blue) compared to the continuous heating of Ref. [9] (red); continuous heating of the rod with structure of Fig. 3 (green). (b) Bond order parameters, Q_4 , Q_6 , W_4 and W_6 , averaged over all atoms internal to the rod, vs. temperature T , for quasi-equilibrium heating of the rod of Fig. 1.

\mathbf{r}_c is the center of mass. In Fig. 2a we plot our results for r_g as the system is heated; the blue curve is for our above “quasi-equilibrium” heating. The vertical dotted lines separate bins of constant temperature simulation, where the temperature is equal to the value at the left end point of the bin; the data plotted within each bin represents the instantaneous value of r_g as a function of increasing time at the constant temperature. At the end of each bin the temperature is increased by a jump of 100 K. We plot our data this way, instead of as an average value at each T , to highlight that significant shape relaxation occurs even at constant T . For comparison, we plot r_g for the continuous heating (red curve) of Ref. [9] for the heating rate of 7×10^{12} K/s; here the temperature is determined from the instantaneous value of the average kinetic energy. We see that the curves are qualitatively similar, with the onset of a plateau around 800 K, however the present quasi-equilibrium heating allows the rod to relax to smaller r_g values, before the rod melts at $T \sim 1200$ K. The decrease in the radius of gyration reflects the shape transformation to a shorter wider rod of smaller aspect ratio.

To investigate the local structure within the cluster, we use the method of bond orientational order parameters [13]. These parameters measure the orientation of bonds connecting a given atom to its nearest neighbors, and provide a convenient means of determining the local crystalline structure of an atom. In particular, we measure the 6-fold and 4-fold orientation parameters, Q_6 , W_6 , Q_4 , and W_4 . We refer the reader to the literature for their definitions [9, 13], and in Table I we give their values for several periodic three dimensional crystal structures. We also, in Table I, give the values of these parameters as computed for atoms on particular low index planar surfaces of an fcc bulk crystal; for these two dimensional parameters we average only over bonds connecting an atom with its neighbors in the specified plane. In Fig. 2b we plot these order parameters for our

TABLE I: Bond order parameters for face-centered-cubic (fcc), hexagonal close-packed (hcp), simple cubic (sc), body-centered-cubic (bcc), and low index fcc planes.

Geometry	Q_4	Q_6	\hat{W}_4	\hat{W}_6
fcc	0.190 94	0.574 52	-0.159 32	-0.013 16
hcp	0.097 22	0.484 76	0.134 10	-0.012 44
sc	0.763 76	0.353 55	0.159 32	0.013 16
bcc	0.082 02	0.500 83	0.159 32	0.013 16
{110}	1	1	0.134 10	-0.093 06
{100}	0.829 16	0.586 30	0.124 97	-0.007 21
{111}	0.375 00	0.740 83	0.134 10	-0.046 26

rod, averaging over only atoms internal to the rod (i.e. we exclude surface atoms since these have fewer nearest neighbor bonds). As for r_g , we plot our data as the instantaneous value as a function of increasing simulation time, for bins of constant temperature (indicated by the dotted vertical lines). Comparing with Table I, we see that the rod maintains its fcc structure until about 400 K. Then, from around 400 K to about 800 K, there is a rise to positive values in \hat{W}_4 , and a decrease in Q_6 and \hat{W}_6 , suggestive of a more hcp-like structure. Above 800 K, the values return to their fcc-like values.

We now focus on the structure of the rod in the high temperature plateau region where r_g stabilizes to a constant. In Fig. 3 we show the configuration of the rod at $T = 900$ K, in the constant plateau region before melting. The views of the rod shown in Figs. 3a,b,c are the same orientations as shown for the initial configuration in Figs. 1a,b,c. In order to better illustrate the order of the rod, we first pick an instantaneous configuration sampled from the middle of the $T = 900$ K simulation, and use the conjugate gradient method [14] to quench local thermal fluctuations. At such high temperatures, the surface can be partially disordered compared to the interior, due to the diffusion of atoms on and near facet edges and vertices [15, 16]. We therefore use the *cone algorithm* [16] to identify and peel away atoms on the surface and in the first sub layer below it, and in Figs. 3a,b show the configuration of the second sub layer of the rod. We see a very regular shape covered almost completely with stable {111} facets. Based on the values in Table I, we use the following criteria to identify atoms in this layer as belonging to particular low index planes: {111} if $0.7 < Q_6 < 0.9$ and $-0.08 < \hat{W}_6 < -0.02$; {100} if $Q_6 < 0.7$ and $\hat{W}_6 > -0.02$; and {110} if $Q_6 > 0.9$ and $\hat{W}_6 < -0.08$. Atoms in Figs. 3a,b have been colored accordingly.

The cross-sectional view in Fig. 3c shows an almost pure fcc interior, as was the case for the initial configuration, however we now see a close packed hexagonal structure characteristic of a {111} plane of the fcc lattice, rather than the {100} plane seen in the cross-sectional

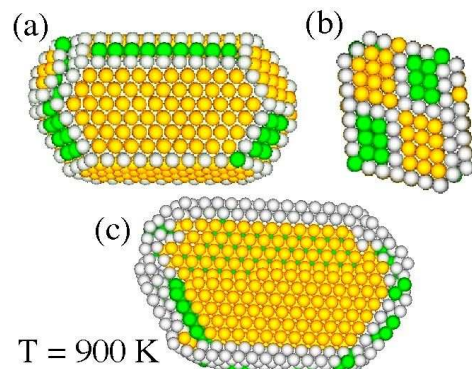


FIG. 3: Configuration of the nanorod after quasi-equilibrium heating to 900 K. (a) side view, and (b) end view down the long axis, after peeling away the surface and the first sub-surface layer; yellow atoms are {111} facets, green atoms are {100} facets, and white are edge atoms. (c) cross-sectional view parallel to the long axis; yellow atoms have a local fcc structure, green atoms have a local hcp structure, and white atoms are neither. The cross-sectional view in (c) shows atoms in the close-packed hexagonal arrangement of a {111} plane of the fcc lattice.

view of Fig. 1c. We thus see one of our main results: in order to align with the new {111} surface facets, the bulk fcc structure has completely reorganized itself to a new orientation. For interior atoms, we use the following criteria to identify the local crystal structure: fcc if $Q_4 > 0.17$ and $\hat{W}_4 < -0.10$; hcp if $Q_4 < 0.13$ and $\hat{W}_4 > 0.07$. Atoms in Fig. 3c have been colored accordingly.

To see how the rod evolves from its initial configuration (Fig. 1) to its reorganized shape (Fig. 3), we consider the average cross-sectional shape in a plane transverse to the long axis of the rod. We compute this average shape as follows. For each instantaneous configuration we first eliminate all atoms on the end caps of the rods, and all interior atoms of the rod, and then project the remaining surface atoms into the xy plane, perpendicular to the long axis of the rod. Placing the origin at the resulting center of mass, we divide the plane into 100 equal polar angles, and then compute the average position of all surface atoms in each angular division. This result is then averaged over 1000 different instantaneous configurations sampled uniformly throughout the simulated time of 43 ns at each temperature T . We plot the resulting average cross-sectional shapes, for several different T , in Fig. 4.

At low T we see the octagonal cross-section of the initially constructed rod of Fig. 1, with the flat edges representing the initial {100} and {110} facets. The shape stays roughly the same until about 400 K. Somewhere between 300 – 400 K, the shape becomes rounder and the initial flat edges disappear. As T increases further, the cross-sectional area grows, representing the shape transformation to a shorter and wider rod of lower aspect ratio,

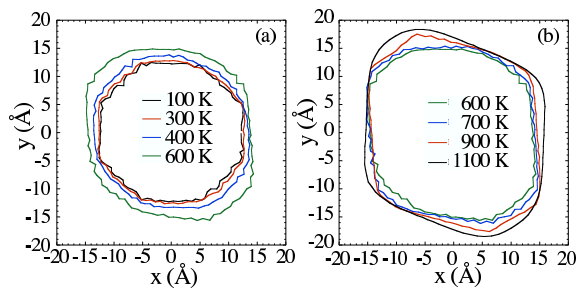


FIG. 4: Average cross-sectional shape, viewed down the long axis of the rod, for different temperatures.

and we see new flat facets develop and grow in new directions. At 900 K we see the fully faceted shape shown in Fig. 3.

In a macroscopic sample, the disappearance of flat facets, with the resulting rounding of the average shape, is a signature of the roughening transition of those surfaces [2]. It is known from experiments that the gold $\{110\}$ surface roughens at 680 K [17], while the $\{100\}$ surface disorders at ~ 1170 K [18], below the bulk melting temperature of 1337 K. In contrast, the macroscopic $\{111\}$ surface is believed to remain stable up to, and even above, the bulk melting [19]. The instability that initiates the shape change which we find in our nanorod at 400 K, may therefore just correspond to the roughening transition of the $\{110\}$ facets, which has been shifted to lower temperature due to large finite size effects in our relatively small rod. After this instability, the surface reorganizes to form mostly lower free energy $\{111\}$ facets, which remain stable until melting. Note that the fully faceted cross-sectional shape at 900 K contains four large sides and two short sides; the former are the $\{111\}$ facets, while the latter are $\{100\}$ facets. By 1100 K, these $\{100\}$ facets have been replaced by a smoothly curved surface. We infer that this is due to the disordering transition of the $\{100\}$ surface, reduced somewhat in temperature due to finite size effects.

In order to see how the interior fcc structure of the rod reorganizes itself to a new orientation, we show in Fig. 5 cross-sectional views of the rod at various temperatures. We color the atoms according to their local crystal structure, using the criteria given above: fcc is yellow, hcp is green, neither is white. Initially, the interior is pure fcc, oriented so that the cross-sectional view shows a $\{100\}$ plane of atoms. As temperature increases, we see that the shape and structural transformation is accompanied by the appearance of hcp planes inside the rod interior, due to the sliding of $\{111\}$ planes. As temperature further increases, the surface becomes less ordered, and more $\{111\}$ planes with different orientation slide. Around 800 K, the surface has reordered and the interior fcc lattice has reoriented so that the cross-sectional view now shows a predominantly $\{111\}$ plane of atoms. At 1100 K, the

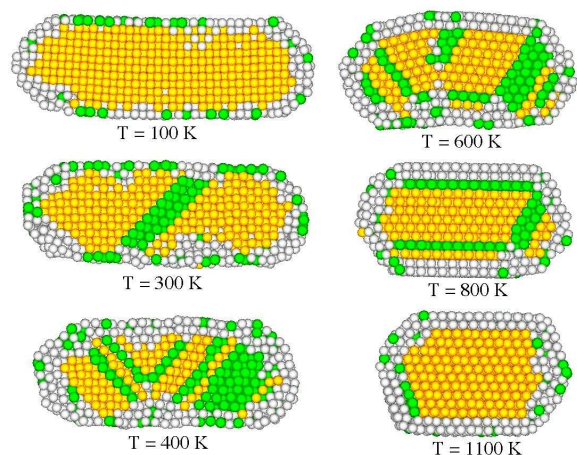


FIG. 5: Cross-sectional view for various temperatures. Atoms are colored according to local crystal structure: fcc is yellow, hcp is green, neither is white.

interior has completely reordered to pure fcc, but with the new orientation.

Such behavior as described above may well exist in other simple elemental metals. We note that many such metals similarly have a roughening transition T_R for the $\{110\}$ surface that is significantly below the bulk melting T_m . Silver, for example, has $T_R = 600$ K and $T_m = 1235$ K, with a similar ratio of T_R/T_m as gold [21]. Lead has $T_R = 415$ K and $T_m = 601$ K, for a somewhat larger T_R/T_m than gold [22].

Finally, in order to verify that instability of the particular surface facets, rather than just the minimization of total surface area, is indeed the mechanism for the shape transformation, we study the stability of a gold nanorod with an aspect ratio of ~ 3 , but with an initial structure similar to that of Fig. 3, with a surface predominantly covered by $\{111\}$ facets. We use a continuous heating MD simulation with a heating rate of 7×10^{12} K/s to model laser heating experiments, for a rod with 3411 atoms. Our results for r_g vs T are shown in Fig. 2a (green curve). Unlike the initial rod of Fig. 1, we now find that the rod remains stable, with no significant shape or structural rearrangement, up until the rod melting temperature. Experiments [23] have shown that nano-sized Pb clusters with large $\{111\}$ surfaces can superheat above melting, consistent with our results. We conclude that the stability of gold, and presumably other metallic, nanorods is crucially dependent upon the structure of the rod surface. Once a shape instability is nucleated, however, the entire bulk of the rod participates in the restructuring.

After our work was completed, we learned of similar work by Diao *et al.* [24] who carried out finite temperature molecular dynamic simulations of gold nanorods, oriented similarly as our initial configuration of Fig. 1, but with a square cross-section and surface covered

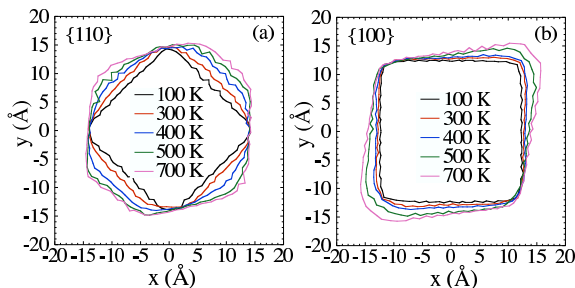


FIG. 6: Average cross-sectional shape viewed down the long axis of the rod, at different temperatures, for (a) a rod initially covered only by $\{110\}$ facets, and (b) a rod initially covered by only $\{100\}$ facets.

entirely by $\{100\}$ facets. Using two different empirical potentials, the “modified embedded atom method” [MEAM] and the “embedded atom method” [EAM] (in contrast to our use of the glue potential), they simulated rods of much larger aspect ratio than considered here. For the MEAM they studied a rod of similar cross-sectional area to ours, but for EAM they used a rod with cross-sectional area roughly one quarter of ours. Despite the different rod shape, aspect ratio, and model potential, they found that, around 300 K, the rod transformed to a shape similar to our Fig. 3, consisting of a rhomboidal cross-section, a surface covered by $\{111\}$ facets, and with the fcc interior having rotated to align with the new facets. For the EAM potential, this transformation occurred by a similar mechanism of sliding $\{111\}$ planes as we have found here. They, however, attribute this transformation to the effects of surface stress on the $\{100\}$ facets.

To clarify whether it is the $\{110\}$ or the $\{100\}$ facets on our initial rod of Fig. 1 that are responsible for the transformation we see, we have carried out new simulations for initial rods of roughly the same cross-sectional area and aspect ratio as in Fig. 1, but now with a square cross-section oriented so that in one case (a) the length of the rod has only $\{110\}$ surface facets (this rod has 2546 atoms), and in a second case (b) the length of the rod has only $\{100\}$ surface facets (this rod has 3126 atoms). Heating for a simulated time of 4.3 ns per temperature with temperature jumps of 100 K, and using the glue potential, we find in both cases a transformation at $T \sim 300 - 400$ K to a similar structure as in Fig. 3, with rotated fcc interior and surface covered primarily by $\{111\}$ facets. In Fig. 6 we show the average cross-sectional areas at different temperatures, computed by the same method as used earlier in Fig. 4, for both these cases (a) and (b). For case (a) of the $\{110\}$ covered rod we see the same rounding out of the $\{110\}$ facets, as the rod begins its transformation to its final shape, as we saw in Fig. 4. For case (b) of the $\{100\}$ covered rod, however, we see no rounding of the facets; rather the corner edges in the $\langle 110 \rangle$ directions round, and the initial $\{100\}$ facets

reorient to $\{111\}$ while remaining perfectly flat. Inspection of the internal structure of the $\{100\}$ covered rod shows that an hcp plane appears as early as $T = 200$ K. By comparing to the results of case (a), we conclude that in our original rod of Fig. 1, it is the $\{110\}$ facets that nucleate the shape transformation, possibly due to the roughening transition of these facets. The results we find for the $\{100\}$ covered rod, however, indicate that more than one mechanism may be important for the transformation of gold nanorods. In all cases, though, the nanorod finds a mechanism to restructure its surface to have stable $\{111\}$ facets dominating, while the interior atoms of the rod participate in this transformation by a reorientation of their initial fcc structure.

This work was funded in part by DOE grant DE-FG02-89ER14017.

-
- [1] J. C. Heyraud and J. J. Métois, *Surf. Sci* **128**, 334 (1983), and *J. Crystal Growth* **50**, 571 (1980).
 - [2] See C. Jayaprakash, W. F. Saam and S. Teitel, *Phys. Rev. Lett.* **50**, 2017 (1983) and references therein.
 - [3] Y. Zhao and B. I. Yakobson, *Phys. Rev. Lett.* **91**, 35501 (2003).
 - [4] J. Diao, K. Gall and M. L. Dunn, *Nat. Mater.* **2**, 656 (2003).
 - [5] Z. L. Wang, M. B. Mohamed, S. Link and M. A. El-Sayed, *Surf. Sci* **440**, L809 (1999).
 - [6] S. Chang, C. Shih, W. Lai and C. R. C. Wang, *Langmuir* **103**, 1165 (1999).
 - [7] S. Link, C. Burda, B. Nikoobakht and M. A. El-Sayed, *J. Phys. Chem B* **104**, 6152 (2000)
 - [8] S. Link, Z. L. Wang and M. A. El-Sayed, *J. Phys. Chem B* **104**, 7867 (2000).
 - [9] Y. Wang and C. Dellago, *J. Phys. Chem. B* **107**, 9214 (2003).
 - [10] F. Ercolessi, M. Parrinello and E. Tosatti, *Philos. Mag. A* **58**, 213 (1988).
 - [11] M. P. Allen, D. J. Tildesley, *Computer Simulation of Liquids* (Clarendon Press, Oxford, 1987).
 - [12] D. J. Evans, W. G. Hoover, B. H. Failor, B. Moran and A. J. C. Ladd, *Phys. Rev. A* **28**, 1016 (1983).
 - [13] P. J. Steinhardt, D. R. Nelson and M. Ronchetti, *Phys. Rev. B* **28**, 784 (1983).
 - [14] W. H. Press, S. A. Teukolsky, W. T. Vetterling and B. P. Flannery, *Numerical Recipes in C: The Art of Scientific Computing* (Cambridge University Press, Cambridge, 1992).
 - [15] Y. Wang, S. Teitel and C. Dellago, *Chem. Phys. Lett.* **394**, 257 (2004).
 - [16] Y. Wang, S. Teitel and C. Dellago, *J. Chem. Phys.* **122**, 214722 (2005).
 - [17] A. Hoss, M. Nold, P. von Blanckenhagen and O. Meyer, *Phys. Rev. B* **45**, 8714 (1992).
 - [18] B. M. Ocko, D. Gibbs, K. G. Huang, D. M. Zehner and S. G. J. Mochrie, *Phys. Rev. B* **44**, 6429 (1991); S. G. J. Mochrie, D. M. Zehner, B. M. Ocko and D. Gibbs, *Phys. Rev. Lett.* **64**, 2925 (1990).
 - [19] K. G. Huang, D. Gibbs, D. M. Zehner, A. R. Sandy and

- S. G. J. Mochrie, Phys. Rev. Lett. **65**, 3313 (1990); G. M. Watson, D. Gibbs, S. Song, A. R. Sandy, S. G. J. Mochrie and D. M. Zehner, Phys. Rev. B **52**, 12329 (1995); P. Carnevali, F. Ercolessi and E. Tosatti, Phys. Rev. B **36**, 6701 (1987).
- [20] Ph. Buffat and J.-P. Borel, Phys. Rev. A **13**, 2287 (1976).
[21] L. Pedemonte and G. Bracco, Surf. Sci. **513** 308, (2002).
[22] H.-N. Yang, T.-M. Lu, and G.-C. Wang, Phys. Rev. Lett. **63**, 1621 (1989).
[23] G. D. T. Spiller, Philos. Mag. A **46**, 535 (1982).
[24] J. Diao, K. Gall and M. L. Dunn, Phys. Rev. B **70**, 1098 (2004).